Effect of electron spin-spin interaction on level crossings and spin flips in a spin-triplet system

Wei Jia,[1,2] Fang-Qi Hu,[1] Ning Wu,[1] and Qing Zhao[1,*]
[1]*Center for Quantum Technology Research, School of Physics, Beijing Institute of Technology, Beijing 100081, China*
[2]*Southwest Institute of Technical Physics, Chengdu 610041, China*
(Received 31 May 2017; published 15 December 2017)

We study level crossings and spin flips in a system consisting of a spin-1 (an electron spin triplet) coupled to a nuclear spin of arbitrary size K, in the presence of a uniform magnetic field and the electron spin-spin interaction within the triplet. Through an analytical diagonalization based on the SU(3) Lie algebra, we find that the electron spin-spin interaction not only removes the curious degeneracy which appears in the absence of the interaction, but also produces some level anticrossings (LACs) for strong interactions. The real-time dynamics of the system shows that periodic spin flips occur at the LACs for arbitrary K, which might provide an option for nuclear or electron spin polarization.

DOI: 10.1103/PhysRevA.96.062507

I. INTRODUCTION

The phenomena of level crossings play an important role in a variety of quantum mechanical systems [1,2], which date back to early works of Hamilton [3], von Neumann and Wigner [4], and Landau and Zener [5,6]. These considerations led to various interesting results, including Berry's phase [7,8], the Hanle effect [9], and so on. More recent topics involving level crossings include quantum phase transitions [10,11], quantum entanglement [12], the Feshbach resonance [13], and electron gases [14]. In particular, the level crossing phenomena can generally appear in the magnetic resonance of atoms or molecules by adjusting an external field, a quantum number, or a coupling constant between submolecular constituents.

As a prototypical model for magnetic resonance, the Breit-Rabi Hamiltonian [15] describes the hyperfine interaction between an electron spin and a nuclear spin, as well as their Zeeman coupling to the external magnetic field [16–19]. In particular, for the Breit-Rabi Hamiltonian with a spin-1 coupled to a nuclear spin with size K, a curious degeneracy with $2K+1$ level crossings is shown to occur at a fixed magnetic field when the nuclear Zeeman splitting is ignored [20,21]. Specifically, the Hamiltonian

$$\hat{H}(x) = x(K+1/2)\hat{S}_z + \hat{\mathbf{K}}\cdot\hat{\mathbf{S}}$$

has been studied in Refs. [20,22], which describes the exchange interaction of two spins $\hat{\mathbf{S}}$ and $\hat{\mathbf{K}}$, with a Zeeman splitting for spin $\hat{\mathbf{S}}$ included. Here $S=1$ and K can be arbitrary and x represents a dimensionless magnetic field. It was found [20] that there is always a nontrivial degeneracy at $x=\pm 1.0$ for arbitrary K (Fig. 1). The degeneracy has shown up as resonances in the spin relaxation rate and has provided key evidence for the particular mechanism of spin relaxation [22]. Bai *et al.* used the Yangian algebra to explain the emergence of such a curious degeneracy in the spin-1 system [23,24].

However, for an electron spin-triplet system, the electron spin-spin interaction plays an essential role, which will greatly affect the properties of system. In recent years, the nitrogen-vacancy (NV) center in diamond has attracted much attention due to the system's long coherence time [25–27]. Such a system is described by the spin-1 Breit-Rabi Hamiltonian with the electron spin-spin interaction included [28–30]. Based on this system, excited-state spectroscopy [31] and dynamic polarization [32] have been studied in a ^{15}NV center coupled to a nuclear spin with $K=1/2$. It is also proposed to enhance the optical readout fidelity in the ^{14}NV center with a $K=1$ nuclear spin [33]. Thus, the spin-1 Breit-Rabi Hamiltonian with arbitrary nuclear spin K and with electron spin-spin interaction included deserves further theoretical study in order to better understand the evolution of the level (anti)crossing and the associated spin relaxations.

In this work, we consider a spin-1 Breit-Rabi Hamiltonian with the electron spin-spin interaction included and at the same time allowing for arbitrary size of K. We will focus on the influence of electron spin-spin interaction on the lifting of the original curious level crossings. By using the fact that the total magnetization along the z axis of the hybrid spin system is conserved, we employ an analytical diagonalization procedure based on the SU(3) Lie algebra to obtain explicit expressions for the eigenvalues. The discriminant method developed in Refs. [34,35] is used as an auxiliary tool to probe the level crossings of the system. It is found that the electron spin-spin interaction removes the original curious degeneracy and generates other level crossings near this point in the weak spin-spin coupling regime. As the spin-spin interaction strength increases, the level crossings develop into level anticrossings (LACs) at some magnetic fields, which has been shown to be relevant to the dynamic polarization of nuclear spin at a certain magnetic field in a NV center [32,33]. The number of LACs is found to be $2K-1$ and originates from the fact that the sum of the eigenenergies in each block is a constant that depends on the hyperfine coupling strength only.

We also study the time evolution of the system and find that perfect periodic spin flips appear at the LACs for arbitrary nuclear spin. In particular, the LACs at or near the zero vertical magnetic field will lead to periodic spin flips, for which the average spin $\langle S_z\rangle$ of the electron changes between -1 and 1. The corresponding states of the nuclear spin will change between $|m+1\rangle$ and $|m-1\rangle$, where $|m|\leqslant K-1$. This might provide some new possibilities of nuclear or electron spin polarization.

The rest of the paper is organized as follows. In Sec. II, the model and methodology are introduced. In Sec. III, the energy

*qzhaoyuping@bit.edu.cn

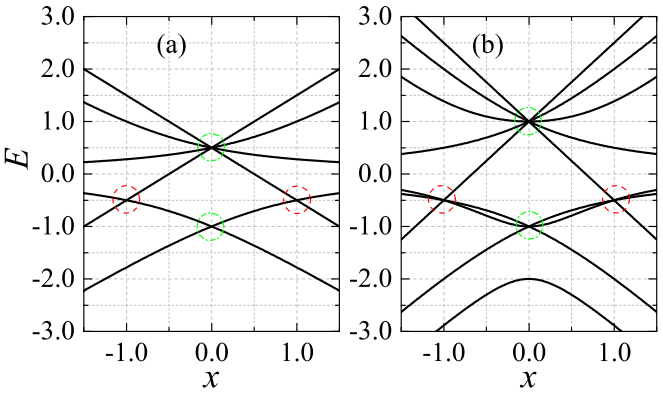

FIG. 1. Energy levels of $\hat{H}(x) = x(K+1/2)\hat{S}_z + \hat{\mathbf{K}}\cdot\hat{\mathbf{S}}$ for $S = 1$ and two different K: (a) $K = 1/2$ and (b) $K = 1$. Note the nontrivial level crossing at $x = \pm 1.0$, which is independent of K.

spectrum is studied in a uniform vertical magnetic field. In Sec. IV, the spin dynamics is presented and analyzed. Finally, we summarize the main results in Sec. V.

II. MODEL

We consider a spin-1 or a triplet formed by an electron spin pair $\hat{\mathbf{S}}_1$ and $\hat{\mathbf{S}}_2$, which is coupled to a nuclear spin $\hat{\mathbf{K}}$ of arbitrary size K via the Heisenberg hyperfine interaction. We also include the electron spin-spin interaction that arises from the magnetic dipole interaction between $\hat{\mathbf{S}}_1$ and $\hat{\mathbf{S}}_2$. By neglecting the Zeeman splitting of the nuclear spin, the system in the presence of a uniform magnetic field $\mathbf{B}$ is described by the Hamiltonian

$$\hat{H} = \xi\hat{\mathbf{K}}\cdot\hat{\mathbf{S}} + \hat{\mathbf{S}}\cdot\mathbf{D}\cdot\hat{\mathbf{S}} + g_s\mu_B\mathbf{B}\cdot\hat{\mathbf{S}}, \tag{1}$$

where ξ is the hyperfine coupling constant and g_s is the g factor of an electron (with μ_B the Bohr magneton). Here $\mathbf{D}$ is a 3×3 matrix and is called the zero-field splitting tensor [36,37]. Its general form depends on the axis frame of the system. For the principal-axis system, it can be chosen to be diagonal as $\mathrm{diag}[D_x, D_y, D_z]$ [36,37]. By choosing a uniform magnetic field $\mathbf{B} = B_0\vec{e}_z$ along the z axis, the Hamiltonian (1) can be made dimensionless by the rescaling $\hat{H}/g_s\mu_B B^* \to \hat{H}_0$,

$$\hat{H}_0 = \lambda_{B_0}\hat{S}_z + \lambda_\xi\hat{\mathbf{K}}\cdot\hat{\mathbf{S}} + \lambda_D\left(\hat{S}_z^2 - \frac{\hat{S}^2}{3}\right) + \lambda_E\left(\hat{S}_x^2 - \hat{S}_y^2\right), \tag{2}$$

where $\lambda_{B_0} = B_0/B^*$, $\lambda_\xi = \xi/g_s\mu_B B^*$, $\lambda_D = D/g_s\mu_B B^*$, and $\lambda_E = E/g_s\mu_B B^*$ are dimensionless parameters with B^* a unit magnetic field. We choose $D = 3D_z/2$ and $E = (D_x - D_y)/2$ as the axial and nonaxial coefficients [37–40], which makes $\mathbf{D}$ traceless.

We define the total spin operator $\hat{\mathbf{J}} = \hat{\mathbf{S}} + \hat{\mathbf{K}}$ of the triplet and the nuclear spin and denote by $|m_S, m_K\rangle$ the basis states $|S, m_S\rangle \otimes |K, m_K\rangle$, where $|S, m_S\rangle$ ($|K, m_K\rangle$) is the eigenstate of $\hat{\mathbf{S}}^2$ and $\hat{S}_z$ ($\hat{\mathbf{K}}^2$ and $\hat{K}_z$). The eigenvalue $m = m_S + m_K$ of $\hat{J}_z$ can take values of $-K-1, -K, \ldots, K$, and $K+1$. It can be easily seen that the total magnetization $\hat{J}_z$ is conserved for $\lambda_E = 0$. However, for $\lambda_E \neq 0$, the Hamiltonian $\hat{H}_0$ no longer commutes with $\hat{J}_z$. Since in many cases $|D| \gg |E|$ [28–30], we henceforth neglect the last term in Eq. (2). The so obtained model has been used to describe a NV center in diamond when $K = 1/2$ [32,41].

For a fixed magnetization $J_z = m$ with $|m| \leqslant K-1$, the Hamiltonian H_0 can be written in the bases $\alpha_1 = |1, m-1\rangle$, $\alpha_2 = |0, m\rangle$, and $\alpha_3 = |-1, m+1\rangle$ as a 3×3 block

$$\hat{H}_0|_{|m|\leqslant K-1} = \begin{pmatrix} b_{m-1} + \frac{\lambda_D}{3} & a_m & 0 \\ a_m & -\frac{2\lambda_D}{3} & c_m \\ 0 & c_m & -b_{m+1} + \frac{\lambda_D}{3} \end{pmatrix}, \tag{3}$$

where

$$a_m = \lambda_\xi\sqrt{(K+m)(K-m+1)/2}, \tag{4}$$

$$b_m = \lambda_{B_0} + \lambda_\xi m, \tag{5}$$

$$c_m = \lambda_\xi\sqrt{(K-m)(K+m+1)/2}. \tag{6}$$

In addition, the Hamiltonian (2) also has two 2×2 blocks for $|m| = K$ and two 1×1 blocks for $|m| = K+1$:

$$\hat{H}_0|_{m=K} = \begin{pmatrix} b_{K-1} + \frac{\lambda_D}{3} & a_K \\ a_K & -\frac{2\lambda_D}{3} \end{pmatrix}, \tag{7}$$

$$\hat{H}_0|_{m=-K} = \begin{pmatrix} -\frac{2\lambda_D}{3} & c_{-K} \\ c_{-K} & -b_{-K+1} + \frac{\lambda_D}{3} \end{pmatrix}, \tag{8}$$

$$\hat{H}_0|_{m=K+1} = b_K + \frac{\lambda_D}{3}, \tag{9}$$

$$\hat{H}_0|_{m=-K-1} = -b_{-K} + \frac{\lambda_D}{3}. \tag{10}$$

The block structure of the total Hamiltonian $\hat{H}_0$ makes it convenient to study the system for arbitrary nuclear spin K.

III. METHODOLOGY

In this work, an algebraic method of SU(3) Lie algebra is used to diagonalize the 3×3 block Hamiltonian $\hat{H}_0|_{|m|\leqslant K-1}$ for a fixed m. Using the eight generators of the SU(3) group in its elementary representation

$$\begin{aligned} I_+ &= \begin{bmatrix} 0 & 1 & 0 \\ 0 & 0 & 0 \\ 0 & 0 & 0 \end{bmatrix}, \quad I_- = \begin{bmatrix} 0 & 0 & 0 \\ 1 & 0 & 0 \\ 0 & 0 & 0 \end{bmatrix}, \\ U_+ &= \begin{bmatrix} 0 & 0 & 0 \\ 0 & 0 & 1 \\ 0 & 0 & 0 \end{bmatrix}, \quad U_- = \begin{bmatrix} 0 & 0 & 0 \\ 0 & 0 & 0 \\ 0 & 1 & 0 \end{bmatrix}, \\ V_+ &= \begin{bmatrix} 0 & 0 & 1 \\ 0 & 0 & 0 \\ 0 & 0 & 0 \end{bmatrix}, \quad V_- = \begin{bmatrix} 0 & 0 & 0 \\ 0 & 0 & 0 \\ 1 & 0 & 0 \end{bmatrix}, \\ I_3 &= \frac{1}{2}\begin{bmatrix} 1 & 0 & 0 \\ 0 & -1 & 0 \\ 0 & 0 & 0 \end{bmatrix}, \quad I_8 = \frac{1}{3}\begin{bmatrix} 1 & 0 & 0 \\ 0 & 1 & 0 \\ 0 & 0 & -2 \end{bmatrix}, \end{aligned} \tag{11}$$

the block Hamiltonian (3) can be written as

$$\begin{aligned} \hat{H}_0|_{|m|\leqslant K-1} &= a_m(I_+ + I_-) + c_m(U_+ + U_-) \\ &\quad + g_m I_3 + h_m I_8 - \frac{2\lambda_\xi}{3}\mathbf{1}, \end{aligned} \tag{12}$$

where

$$g_m = b_m - \lambda_\xi + \lambda_D,$$
$$h_m = (3b_m + \lambda_\xi - \lambda_D)/2 \tag{13}$$

and **1** is the 3×3 unit matrix. It is well known that the eight generators given by Eq. (11) can be classified into three angular momentum operators I_+, I_-, and I_3, which form the SU(2) subalgebra, and five quadrupole operators $U_\pm$, $V_\pm$, and I_8 [42]. Equations (12) and (13) indicate that the effect of the spin-spin interaction is included in terms proportional to the two Cartan operators I_3 and I_8.

According to standard Lie algebraic theory [43–45], a Hermitian operator that is a linear function of the N generators of a compact semisimple Lie group can be transformed into a linear combination of the Cartan operators of the corresponding Lie algebra by the transformation

$$\hat{H}_0 \to \hat{H}_0' = W\hat{H}_0 W^{-1}, \quad W = \prod_{i=1}^{N} \exp(x_i C_i), \tag{14}$$

where $\{C_i\}$ $(i = 1, \ldots, N)$ is a basis set in the Cartan standard form of the semisimple Lie algebra and x_i is the corresponding coefficients to be determined. Here we choose

$$W = e^{x_5 V_+} e^{x_2 I_-} e^{x_4 U_-} e^{x_1 I_+} e^{x_3 U_+} e^{x_6 V_-}. \tag{15}$$

Note that x_i can be set equal to zero if the corresponding C_i is a Cartan operator (an element of the Cartan subalgebra) [45]. After a straightforward calculation, we have the following diagonal form of the transformed Hamiltonian:

$$\hat{H}_0'|_{|m|\leqslant K-1} = g_m' I_3 + h_m' I_8 - \frac{2\lambda_\xi}{3}\mathbf{1}, \tag{16}$$

with

$$g_m' = g_m + (2a_m x_1 - c_m x_3),$$
$$h_m' = h_m + 3c_m x_3/2, \tag{17}$$

where the coefficients x_1 and x_3 are determined by solving the algebraic equations

$$c_m - a_m x_6 + \left(\tfrac{1}{2}g_m - h_m\right)x_3 - c_m x_3^2 = 0,$$
$$\left(h_m + \tfrac{1}{2}g_m\right)x_6 + (a_m + c_m x_6)x_3 = 0, \tag{18}$$
$$a_m + c_m x_6 - (g_m - c_m x_3)x_1 - a_m x_1^2 = 0.$$

Note that Eq. (17) only involves the two variables x_1 and x_3, though x_2, x_4, and x_5 can be solved by another three coupled equations. In the following, we will omit the subindex m in the variables a_m, b_m, c_m, g_m, and h_m for simplicity.

There are six sets of solutions (x_1, x_3, x_6) of Eq. (18), which are permutations of the particular solution

$$x_1 = (-4ch - 6cg + \sqrt{3}acf + \Lambda_k)/12ac,$$
$$x_3 = \frac{1}{6c^2}(-4ch + \Lambda_k), \tag{19}$$
$$x_6 = [36c^4 + 4c^2h(2h - 3g) + (3gc + 2hc)\Lambda_k - \Lambda_k^2]/36ac^3,$$

where

$$f = \sqrt{[e - 8ch(-4ch + \Lambda_k) - (-4ch + \Lambda_k)^2]/a^2c^2},$$
$$\Lambda_k = (k_1 - \sqrt{k_2})^{1/3} + (k_1 + \sqrt{k_2})^{1/3},$$
$$e = 48a^2c^2 + 48c^4 + 12c^2g^2, \tag{20}$$
$$k_1 = 54c^5 g - 72a^2c^3 h + 36c^5 h - 18c^3 g^2 h + 8c^3 h^3,$$
$$k_2 = c^6\{-(12a^2 + 12c^2 + 3g^2 + 4h^2) + 4[36a^2 h + 9g^2 h - 4h^3 - 9c^2(3g + 2h)]^2\}.$$

Note that any other solution as a permutation of the particular solution given by Eq. (19) only results in a rearrangement of the diagonal elements in H_0' and hence does not affect any physical result. We thus analytically obtain all the eigenvalues of $\hat{H}_0$:

$$U_1^{(|m|\leqslant K-1)} = \frac{g}{2} + \frac{h}{3} + ax_1 - \frac{2\lambda_\xi}{3},$$
$$U_2^{(|m|\leqslant K-1)} = -\frac{g}{2} + \frac{h}{3} - ax_1 + cx_3 - \frac{2\lambda_\xi}{3},$$
$$U_3^{(|m|\leqslant K-1)} = -\frac{2}{3}h - cx_3 - \frac{2\lambda_\xi}{3},$$
$$U_1^{(m=K)} = \frac{1}{6}(4b - g - 3\sqrt{4a^2 + g^2}) - \frac{2\lambda_\xi}{3},$$
$$U_2^{(m=K)} = \frac{1}{6}(4b - g + 3\sqrt{4a^2 + g^2}) - \frac{2\lambda_\xi}{3}, \tag{21}$$
$$U_1^{(m=-K)} = \frac{1}{6}(-2b - g - 3\sqrt{4b^2 + 4c^2 - 4bg + g^2}) - \frac{2\lambda_\xi}{3},$$
$$U_2^{(m=-K)} = \frac{1}{6}(-2b - g + 3\sqrt{4b^2 + 4c^2 - 4bg + g^2}) - \frac{2\lambda_\xi}{3},$$
$$U^{(m=K+1)} = \frac{1}{3}(2b + g) - \frac{2\lambda_\xi}{3},$$
$$U^{(m=-K-1)} = \frac{1}{3}(-4b + g) - \frac{2\lambda_\xi}{3}.$$

It is worth pointing out that the transformation W given by Eq. (15) is not a unitary one and hence we can only get the eigenvalues rather than the eigenvectors of the system. However, as we will see, these analytical expressions for the eigenvalues are beneficial to the analysis of the evolution of the energy spectrum.

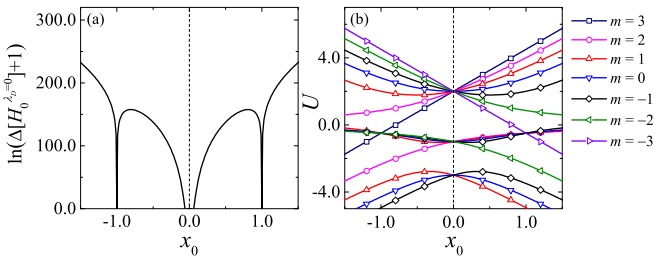

FIG. 2. (a) Plot of $\ln(\Delta[\hat{H}_0^{\lambda_D=0}] + 1)$, the logarithmic representation of the discriminant of $\hat{H}_0$ when $\lambda_D = 0$. (b) Spectrum as a function of the rescaled dimensionless magnetic field x_0. The other parameters are $K = 2$, $\nu = 0.5$, $\lambda_\xi = 1.0$, and $\lambda_D = 0$.

IV. RESULTS

A. Weak spin-spin interaction

In this section, we set $\lambda_\xi = 1.0$ and $\lambda_{B_0} = x_0(K+\nu)$ in the Hamiltonian (2), with ν a constant and x_0 a rescaled dimensionless magnetic field. Let us first focus on the case of $S = 1$ and $K = 2$, for example, in the case of the ^{87}Rb vapor studied in Ref. [22].

In order to see the effect of spin-spin interaction on the energy spectrum, we first study the case of $\lambda_D = 0$ by using the discriminant method [34,35]. The discriminant $\Delta[\hat{H}_0^{\lambda_D=0}]$ of $\hat{H}_0$ reads

$$\begin{aligned}\Delta\big[\hat{H}_0^{\lambda_D=0}\big] = {} & 36520347436056576\lambda_{B_0}^{68}\big(5-2\lambda_{B_0}\big)^{20}\big(5+2\lambda_{B_0}\big)^{20}\big(9-2\lambda_{B_0}+\lambda_{B_0}^2\big)\big(9+2\lambda_{B_0}+\lambda_{B_0}^2\big)\\ & \times\big(225+139\lambda_{B_0}^2+16\lambda_{B_0}^4+\lambda_{B_0}^6\big)\big(900-1000\lambda_{B_0}+875\lambda_{B_0}^2-324\lambda_{B_0}^3+112\lambda_{B_0}^4-24\lambda_{B_0}^5+4\lambda_{B_0}^6\big)\\ & \times\big(900+1000\lambda_{B_0}+857\lambda_{B_0}^2+324\lambda_{B_0}^3+112\lambda_{B_0}^4+24\lambda_{B_0}^5+4\lambda_{B_0}^6\big),\end{aligned} \tag{22}$$

whose zeros determine the level crossing points in the spectrum. It is easy to see that the equation $\Delta[\hat{H}_0^{\lambda_D=0}] = 0$ has real solutions $\lambda_{B_0} = 0$ and $\lambda_{B_0} = \pm 2.5$, which correspond to the degeneracies at $x_0 = 0$ and $x_0 = \pm 1.0$ for $\nu = 0.5$, respectively [Fig. 2(a)]. The dips represent the level crossings. Energy eigenvalues calculated by Eq. (21) are shown in Fig. 2(b) as functions of the dimensionless magnetic field x_0. Due to the conservation of the total magnetization, each energy level is labeled by a quantum number m. There are three degenerate energies at $x_0 = 0$, namely, $U = -3.0$ (for $m = -1$, 0, and 1), $U = -1.0$ (for $m = -2$, -1, 0, 1, and 2), and $U = 2.0$ (for $m = -3$, -2, -1, 0, 1, 2, and 3). Of particular interest is the degeneracy at $x_0 = +1.0$ with energy $U = -1/2$, where the energy levels corresponding to $m = -3$, -1, 0, 1, and 2 are crossed. These degeneracies were revealed in Ref. [22] and discussed in detail in Refs. [20,23].

In general, the degeneracy point $x_0^*(\nu, K)$ is a function of both ν and K. Actually, by setting the eigenenergies in the $m = -K-1$ and $m = K$ ($m = K+1$ and $m = -K$) blocks equal, one can find

$$x_0^*(\nu, K) = \pm\frac{K+0.5}{K+\nu}. \tag{23}$$

Note that for $\nu = 0.5$, the degeneracy at $x_0 = \pm 1.0$ holds for arbitrary K (Fig. 3). However, the degenerate energy is still $U = -1/2$ and does not depend on the values of ν or K. In contrast, the three degenerate energies at $x_0^* = 0$ are $U = K$, $U = -1$, and $U = -K-1$, respectively, which depend on the value of K only. In the following, we will set $\nu = 0.5$.

When the spin-spin interaction is present, the original degeneracies at $x_0 = 0$ and $x_0 = \pm 1.0$ are lifted. Figure 4(a) shows the energy spectrum of H_0 for a finite spin-spin interaction $\lambda_D = 0.4$ and $K = 2$. It can be seen that new level crossings appear around $x_0 = 0$ and $x_0 = \pm 1$ [Figs. 4(b) and 4(d)]. The behavior of the discriminant reflecting the level crossings is shown in Fig. 4(c). Thus, weak spin-spin interactions remove the original degeneracy and develop new level crossings around the degenerate points.

B. Strong spin-spin interaction

In this section, we consider strong spin-spin interaction with $\lambda_D > \lambda_\xi$, which is the case of a NV center in diamond [28,29]. In the case of $\lambda_\xi = 0$, the electronic and nuclear spins are decoupled and the eigenenergies of the electron pair are simply given by $U_1 = \lambda_D/3 - \lambda_{B_0}$, $U_2 = \lambda_D/3 + \lambda_{B_0}$, and $U_3 = -2\lambda_D/3$ [Fig. 5(a)], which correspond to the three states $|-1\rangle$, $|1\rangle$, and $|0\rangle$ in the triplet, respectively.

Figure 5(b) shows the energy spectrum for a strong spin-spin interaction $\lambda_D = 10.0$, which has an outline similar to that in Fig. 5(a), but with fine structures arising from the hyperfine coupling. It is clear that the level crossings at $x_0 = 0$ and $x_0 \simeq \pm 6.67$ in Fig. 5(a) evolve into some LACs and new level crossings in Fig. 5(b) due to the presence of the electron-nuclear spin coupling. In order to analyze the level (anti)crossings, we calculate the discriminant $\Delta[\hat{H}_0]$ for general λ_D,

$$\begin{aligned}\Delta[\hat{H}_0] = {} & 4069\lambda_{B_0}^6\big(\lambda_{B_0}-\lambda_D\big)^2\big(\lambda_{B_0}+\lambda_D\big)^2\big(-3\lambda_{B_0}+2\lambda_{B_0}^2+\lambda_D-2\lambda_{B_0}\lambda_D\big)^2\big(-3\lambda_{B_0}+2\lambda_{B_0}^2+2\lambda_D-2\lambda_{B_0}\lambda_D\big)^2\\ & \times\big(3\lambda_{B_0}+2\lambda_{B_0}^2+\lambda_D+2\lambda_{B_0}\lambda_D\big)^2\big(3\lambda_{B_0}+2\lambda_{B_0}^2+2\lambda_D+2\lambda_{B_0}\lambda_D\big)^2\big(4+\lambda_{B_0}^2-2\lambda_{B_0}\lambda_D+\lambda_D^2\big)\\ & \times\big(4+\lambda_{B_0}^2+2\lambda_{B_0}\lambda_D+\lambda_D^2\big)\big(3\lambda_{B_0}^2+2\lambda_{B_0}^3+2\lambda_{B_0}\lambda_D-4\lambda_{B_0}^2\lambda_D-\lambda_D^2+2\lambda_{B_0}\lambda_D^2\big)^2\\ & \times\big(-3\lambda_{B_0}^2+2\lambda_{B_0}^3+2\lambda_{B_0}\lambda_D+4\lambda_{B_0}^2\lambda_D+\lambda_D^2+2\lambda_{B_0}\lambda_D^2\big)^2\\ & \times\big(9+23\lambda_{B_0}^2+4\lambda_{B_0}^4+\lambda_{B_0}^6-2\lambda_D-24\lambda_{B_0}^2\lambda_D+4\lambda_{B_0}^4\lambda_D+\lambda_D^2+16\lambda_{B_0}^2\lambda_D^2-2\lambda_{B_0}^4\lambda_D^2-4\lambda_{B_0}^2\lambda_D^3+\lambda_{B_0}^2\lambda_D^4\big).\end{aligned} \tag{24}$$

The dips appearing in Fig. 5(c) correspond to the level crossings. In addition, we note that the two levels in the $m = 0$ sector develop a LAC at $x_0 = 0$ [inset of Fig. 5(b)]. In fact, when $\Delta[\hat{H}_0] = 0$ is solved for $\lambda_D = 10.0$, only the last factor on the right-hand side of Eq. (24) has pure imaginary solutions, which implies the appearance of LAC at $x_0 = 0$. In general, the number of LACs around $x_0 = 0$ depends on the value of K. For general values of K, there are $2K-1$ LACs distributed

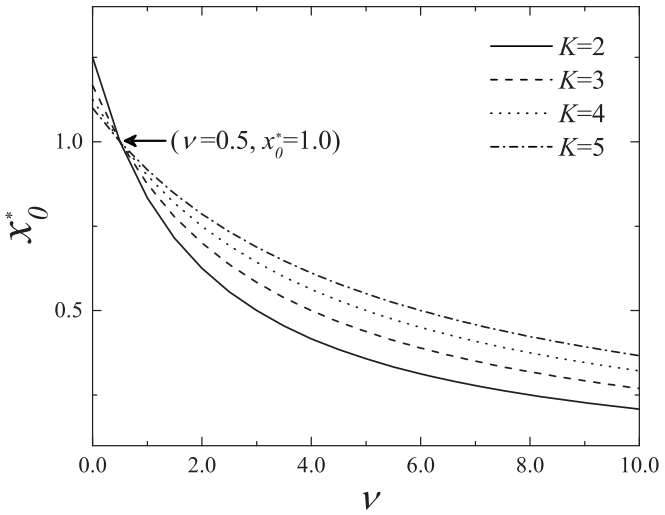

FIG. 3. Relationship between ν and x_0^* for different K, where $\lambda_\xi = 1.0$ and $\lambda_D = 0$.

symmetrically with respect to $x_0 = 0$, each resulting from a pair of states in the m sector for $|m| \leqslant K - 1$. Figure 5(d) shows the structures of the LACs for $K = 3/2$ and $K = 3$. Actually, it can be seen from Eq. (21) that the sum of the three eigenenergies in the m sector with $|m| \leqslant K - 1$ is a constant,

$$\sum_{i=1}^{3} U_i^{(|m|\leqslant K-1)} = -2\lambda_\xi, \tag{25}$$

which is independent of K and m, as well as all other system parameters except for λ_ξ. As an illustration, we show in Fig. 6(a) the three ordered eigenenergies $U_T \geqslant U_M \geqslant U_B$ at $x_0 = 0$ for $K = 1$ and $m = 0$, as functions of the electron spin-spin coupling λ_D. It can be seen that as $|\lambda_D|$ increases, two of the three eigenenergies become closer to each other and result in a LAC. In order to study other general LACs away from $x_0 = 0$, we define a LAC point by equating the

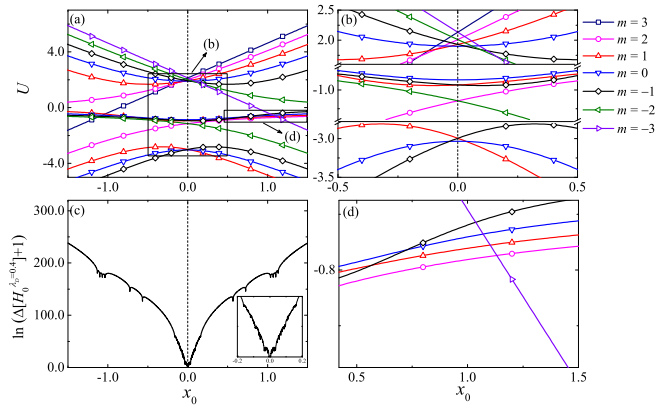

FIG. 4. (a) Spectrum as a function of the rescaled dimensionless magnetic field x_0 for $\lambda_D = 0.4$. (b) Magnification of the energy spectrum near $x_0 = 0$. (c) Discriminant of $\hat{H}_0$ (the finite height of the dips is due to the limitation of the graphic resolution). (d) Magnification of the energy spectrum near $x_0 = 1.0$. The other parameters are $K = 2$, $\nu = 0.5$, $\lambda_D = 0.4$, and $\lambda_\xi = 1.0$.

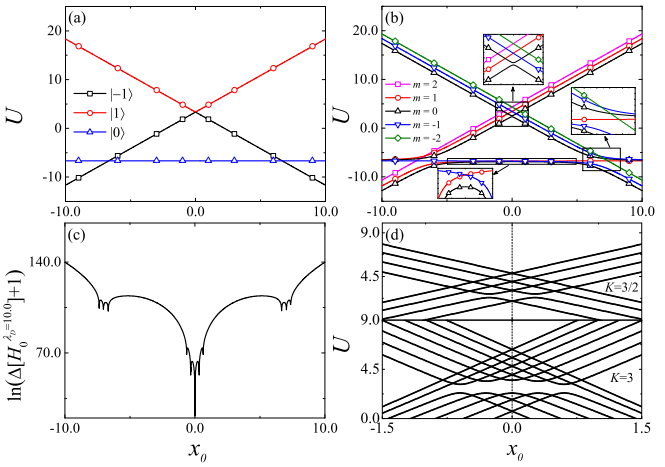

FIG. 5. Spectrum as a function of the rescaled dimensionless magnetic field x_0 for (a) $K = 1$, $\nu = 0.5$, $\lambda_\xi = 0$, and $\lambda_D = 10.0$ and (b) $K = 1$, $\nu = 0.5$, $\lambda_\xi = 1.0$, and $\lambda_D = 10.0$. (c) Discriminant of $\hat{H}_0$ when $K = 1$, $\nu = 0.5$, $\lambda_\xi = 1.0$, and $\lambda_D = 10.0$. (d) The LACs around $x_0 = 0$ for different K.

slopes of two relevant eigenenergies with respect to x_0 for each fixed m, i.e.,

$$\frac{\partial U_i^{(m)}}{\partial x_0} = \frac{\partial U_j^{(m)}}{\partial x_0}, \tag{26}$$

where i and j label the two eigenenergies involved. Thus, a LAC is also the point at which the energy gap between the two states reaches a minimum. For example, for $K = 1$, the LACs in the $m = \pm 1$ sectors are calculated to be $x_0 = \mp 6.667$, while there are three LACs in the $m = 0$ sector at $x_0 = 0$ and ± 6.036 [Fig. 6(b) and the inset of Fig. 5(b)].

V. SPIN DYNAMICS

In this section, we study the real-time dynamics of the hybrid electron-nuclear spin system. Due to the conservation of the total magnetization m, we solve the time-dependent Schrödinger equation in each m block for given initial states. In addition, $\lambda_\xi = 1.0$ and $\nu = 0.5$ are used in this section.

First, we consider the initial state $|\psi_0\rangle = |0, -K\rangle$ so that the dynamics is described by the 2×2 block Hamiltonian $\hat{H}_0|_{m=-K}$. From Eq. (8), the probabilities $P_{|\chi\rangle}(t) =$

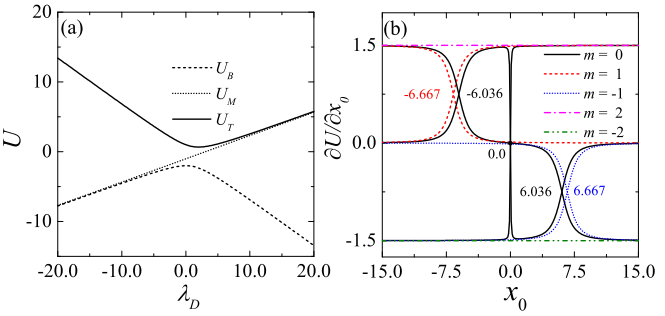

FIG. 6. (a) Spectrum as a function of the coupling strength λ_D at $x_0 = 0$ for $K = 1$ and $m = 0$. (b) Derivative $\partial U/\partial x_0$ for $K = 1$ and $\lambda_D = 10.0$. Here $\lambda_\xi = 1.0$ and $\nu = 0.5$.

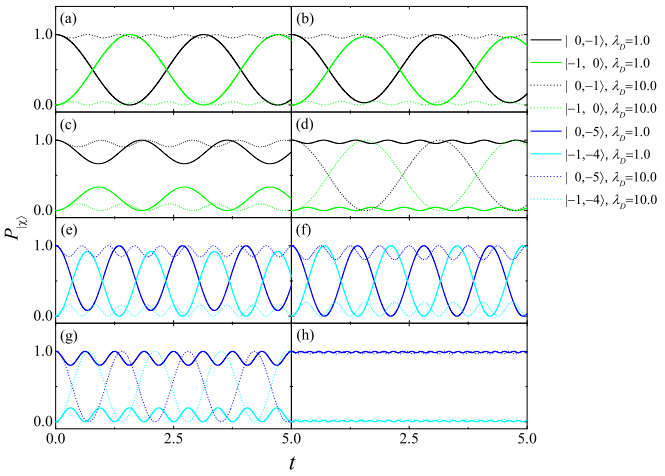

FIG. 7. Evolution of the probability $P_{|\chi\rangle}$ from the initial state $|\psi_0\rangle = |0,-K\rangle$ for (a)–(d) $K = 1$ and (e)–(h) $K = 5$. The solid and dotted curves show the results for $\lambda_D = 1.0$ and 10.0, respectively. The other parameters are $\lambda_\xi = 1.0$, $\nu = 0.5$, and (a) $x_0 = 0.667$, (b) $x_0 = 0.909$, (c) $x_0 = 2.545$, (d) $x_0 = 6.667$, (e) $x_0 = 0.667$, (f) $x_0 = 0.909$, (g) $x_0 = 2.545$, and (h) $x_0 = 6.667$.

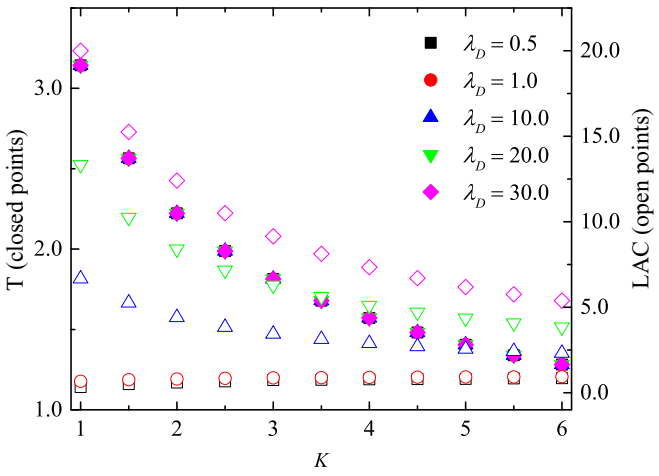

FIG. 8. Variation of the oscillation period of perfect switching between $|0,-K\rangle$ and $|-1,K+1\rangle$ (closed points), and the corresponding LACs (open points) with different K and coupling strength λ_D. The other parameters are $\lambda_\xi = 1.0$ and $\nu = 0.5$.

$|\langle\chi|e^{-i\hat{H}_0 t}|\psi_0\rangle|^2$ of finding the state in $|\chi\rangle = |0,-K\rangle$ and $|-1,-K+1\rangle$ at time t are

$$P_{|-1,-K+1\rangle}(t) = \frac{16K}{A_1}\sin^2\left(\frac{\sqrt{A_1}}{4}t\right), \tag{27}$$

$$P_{|0,-K\rangle}(t) = 1 - P_{|-1,-K+1\rangle}(t), \tag{28}$$

where

$$A_1 = 4\lambda_D^2 + 4K^2(x_0-1)^2 + (x_0+2)^2 + 4K\left(2+x_0+x_0^2\right) - 4\lambda_D[2+2K(x_0-1)+x_0]. \tag{29}$$

Figure 7 shows the time evolution of these probabilities and we find that perfect periodic switchings between $|0,-K\rangle$ and $|-1,-K+1\rangle$ are achieved at the LACs, i.e., $x_0 = 0.667$ (0.909) for $K = 1$ (5) when $\lambda_D = 1.0$ [solid curves in Figs. 7(a) and 7(f)] and $x_0 = 6.667$ (2.545) for $K = 1$ (5) when $\lambda_D = 10.0$ [dotted curves in Figs. 7(d) and 7(g)]. These LACs are determined by substituting the two eigenenergies $U_1^{(m=-K)}$ and $U_2^{(m=-K)}$ into Eq. (26), giving

$$\tilde{x}_0(\nu,K,\lambda_D) = \frac{K-1+\lambda_D}{K+\nu}, \tag{30}$$

which is presented by open points in Fig. 8 for different K and λ_D. The period $T = 4\pi/\sqrt{A_1}$ for the perfect oscillations of $P_{|\chi\rangle}$ at the LACs is also shown by solid points in Fig. 8. It is found that T decreases with increasing K and is independent of the coupling strength λ_D. Actually, by substituting Eq. (30) into Eq. (29), we have $A_1 = 16K$ and hence $T = \pi/\sqrt{K}$. So the amplitude $|16K/A_1|$ for $P_{|\chi\rangle}(t)$ reaches unity at the LACs, which explains the perfect oscillations observed above.

We next consider the initial state $|\psi_0\rangle = |-1,m+1\rangle$ with $|m| \leqslant K-1$. The perfect flip of states will still appear at the LACs. For $K = 1$ and $\lambda_D = 10.0$, there are two LACs for $m = 0$ [see Fig. 6(b)] at $\tilde{x}_0 = \pm 6.036$, which have been noticed before [32,33]. The time evolution of the probabilities in the states $|0,0\rangle$, $|-1,1\rangle$, and $|1,-1\rangle$ at the LAC $\tilde{x}_0 = 6.036$ are shown as dashed curves in Fig. 8(a). The corresponding dynamics for the electron polarization $\langle S_z(t)\rangle = \langle\psi_0|e^{i\hat{H}_0 t}S_z e^{-i\hat{H}_0 t}|\psi_0\rangle$ is shown in Fig. 8(b). It can be seen that $\langle S_z(t)\rangle$ oscillates periodically between -1 and 0. At the LAC point $\tilde{x}_0 = 0$, the evolution of the probabilities is mainly distributed between $|-1,1\rangle$ and $|1,-1\rangle$ [solid curves in Fig. 9(a)]. The dynamics of $\langle S_z(t)\rangle$ shown in Fig. 9(b) indicates that the spin flip occurs between $\langle\hat{S}_z\rangle = -1$ and $\langle\hat{S}_z\rangle = 1$.

Actually, in the $m = 0$ sector and at the LAC $\tilde{x}_0 = 0$, the dynamics of the probabilities of the three states $P_{|1,m-1\rangle}(t)$, $P_{|0,m\rangle}(t)$, and $P_{|-1,m+1\rangle}(t)$ can be obtained analytically (see the Appendix). The corresponding electron polarization $\langle S_z(t)\rangle$

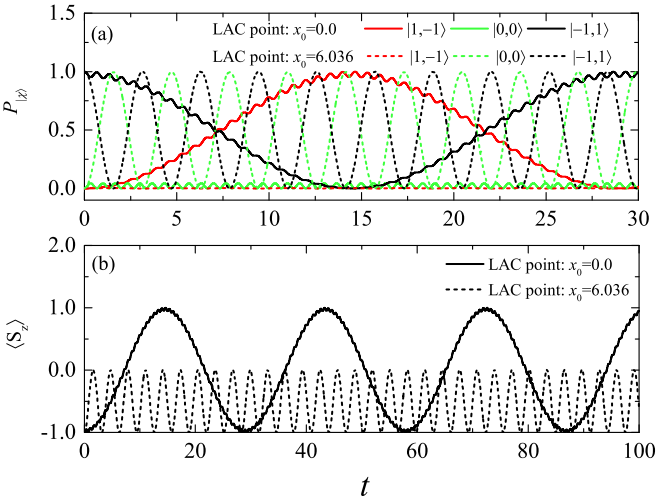

FIG. 9. (a) Evolution of the probability $P_{|\chi\rangle}$ from the initial state $|\psi_0\rangle = |-1,m+1\rangle$ at the LACs $x_0 = 0.0$ (solid curves) and $x_0 = 6.036$ (dashed curves) for $m = 0$. (b) Corresponding dynamics of the electron polarization $\langle S_z(t)\rangle$. The other parameters are $K = 1$, $\lambda_\xi = 1.0$, $\lambda_D = 10.0$, $\nu = 0.5$, and $\lambda_{B_0} = 1.5x_0$.

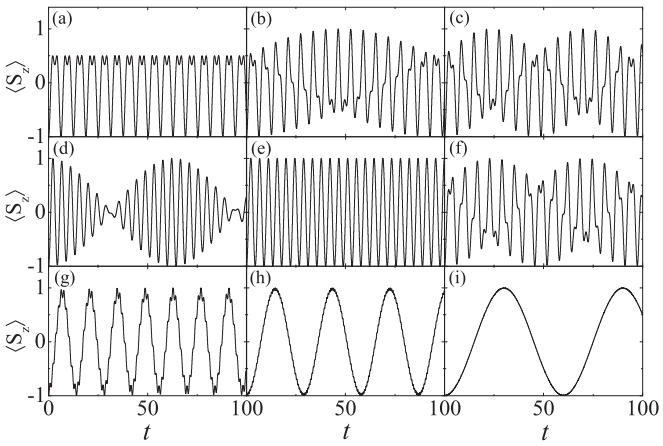

FIG. 10. Dynamics of the electron polarization $\langle \hat{S}_z \rangle$ for different spin-spin coupling strength λ_D. Here $K = 1$, $\lambda_\xi = 1.0$, $x_0 = 0$, $\nu = 0.5$, $\lambda_{B_0} = 1.5x_0$, and (a) $\lambda_D = 0$, (b) $\lambda_D = 0.05$, (c) $\lambda_D = 0.1$, (d) $\lambda_D = 0.9$, (e) $\lambda_D = 1.0$, (f) $\lambda_D = 2.1$, (g) $\lambda_D = 5.0$, (h) $\lambda_D = 10.0$, and (i) $\lambda_D = 20.0$.

reads

$$\langle S_z(t) \rangle = -\frac{1}{2C_1}\left[C_2 \cos\left(\frac{-1+\lambda_D-\sqrt{C_1}}{2}t\right) + C_3 \cos\left(\frac{-1+\lambda_D+\sqrt{C_1}}{2}t\right)\right], \tag{31}$$

where

$$\begin{aligned} C_1 &= (\lambda_D - 1)^2 + 4K + 4K^2, \\ C_2 &= C_1 + (\lambda_D - 1)\sqrt{C_1}, \\ C_3 &= C_1 - (\lambda_D - 1)\sqrt{C_1}. \end{aligned} \tag{32}$$

It can be seen that $\langle S_z(t) \rangle$ generally behaves as a modulated oscillation controlled by both K and λ_D (Fig. 10). In particular, for $\lambda_D = 1.0$ we have $C_1 = C_2 = C_3$ and hence $\langle S_z(t) \rangle = -\cos\sqrt{K(K+1)}t$, which oscillates with a period $T = 2\pi/\sqrt{K(K+1)}$. In addition, in the strong spin-spin coupling regime with $\lambda_D \gg \lambda_\xi, K$, we have $\sqrt{C_1} \approx \lambda_D - 1 + 2\frac{K(K+1)}{\lambda_D - 1}$, so $C_2 \approx 2(\lambda_D - 1)^2 + 6K(K+1)$ and $C_3 \approx 2K(K+1)$. Since $C_2 \gg C_3$, $\langle S_z(t) \rangle$ oscillates almost perfectly with period $T \approx 2\pi \frac{\lambda_D - 1}{K(K+1)}$, which increases with increasing λ_D [see Figs. 10(g)–10(i)].

Previous studies about dynamic polarization of nuclear spins have shown that the strong spin mixing will occur at the LACs in nitrogen-vacancy centers [31,32], which will lead to the precession of a certain frequency in different states. For ^{14}NV with nuclear spin $K = 1$, the LAC of the excited state is at $500Gs$ and leads the precession of nuclear spin states $|1\rangle \leftrightarrows |0\rangle$ [32,33]. The above analysis shows that the similar LACs at $\tilde{x}_0 = 6.667$ for $m = -1$ and at $\tilde{x}_0 = 6.036$ for $m = 0$ also lead to the precession in different states and causes the periodic flip of states or spin flip. In particular, when the system lies in the strong-coupling regime, the LACs at $x_0 = 0$ (for $m = 0$) and near $x_0 = 0$ (for $m \neq 0$) [see Fig. 5(d)] lead to different spin flip between $|m+1\rangle \leftrightarrows |m-1\rangle$, where $|m| \leqslant K - 1$. This may provide a new possible electron or nuclear spin polarization mechanism at or near the zero vertical magnetic field.

VI. CONCLUSION

We studied the static and dynamical properties of a common system consisting of an electron pair of spin-1 and a nuclear spin of arbitrary size. The Zeeman splitting on the electrons, the hyperfine interaction between the electron and nuclear spin, and the electron spin-spin interaction within the pair were considered. Due to the conservation of the total magnetization, the block Hamiltonian within fixed magnetization was diagonalized using an algebraic approach based on the SU(3) Lie algebra, which provides a convenient way for the analysis of the energy spectrum. The discriminant method was employed as an auxiliary tool to probe the level (anti)crossings. It was found that the spin-spin interaction can transform the original curious degeneracy into some nearby LACs. We then studied the real-time dynamics of the composite system and showed that perfect state switching occurs at the LACs for arbitrary nuclear spin. The special spin flip appearing at or near zero magnetic field might shed some light on the electron-nuclear polarization mechanism.

ACKNOWLEDGMENTS

The authors thank Dr. Hong-Biao Zhang and Prof. Mo-Lin Ge for valuable discussions. This work was supported by NSF of China through Grants No. 11675014 and No. 11705007. Additional support was provided by the Ministry of Science and Technology of China (Grant No. 2013YQ030595-3).

APPENDIX

For the arbitrary integer K, the LAC must occur at $\tilde{x}_0 = 0$ for $m = 0$. When the initial state is $|\psi_0\rangle = |-1, m+1\rangle$, the probabilities are

$$P_{|1,-m+1\rangle}(t) = \frac{1}{16C_1^2}\left[4C_1^2 + C_2^2 + C_3^2 - 4C_1C_2 \cos\left(\frac{-1+\lambda_D-\sqrt{C_1}}{2}t\right) - 4C_1C_3 \cos\left(\frac{-1+\lambda_D+\sqrt{C_1}}{2}t\right) + 2C_2C_3 \cos\left(\sqrt{C_1}t\right)\right], \tag{A1}$$

$$P_{|0,m\rangle}(t) = \frac{K(K+1)}{C_1}[1 - \cos(\sqrt{C_1}t)], \tag{A2}$$

and

$$P_{|-1,m+1\rangle}(t) = \frac{1}{16C_1^2}\Bigg[4C_1^2 + C_2^2 + C_3^2 + 4C_1C_2\cos\left(\frac{-1+\lambda_D-\sqrt{C_1}}{2}t\right) + 4C_1C_3\cos\left(\frac{-1+\lambda_D+\sqrt{C_1}}{2}t\right) + 2C_2C_3\cos\left(\sqrt{C_1}t\right)\Bigg], \tag{A3}$$

where C_1, C_2, and C_3 have been defined in the main text. Then the average spin is $\langle S_z(t)\rangle = P_{|1,-m+1\rangle}(t) - P_{|-1,m+1\rangle}(t)$.

[1] W. Nagourney, W. Happer, and A. Lurio, Phys. Rev. A **17**, 1394 (1978).
[2] B. M. Garraway and N. V. Vitanov, Phys. Rev. A **55**, 4418 (1997).
[3] W. R. Hamilton, Dublin Univ. Rev. Q. Mag **1**, 795 (1833).
[4] J. von Neumann and E. P. Wigner, Phys. Z. **30**, 467 (1929).
[5] L. Landau, Phys. Z. Sowjetunion **2**, 46 (1932).
[6] C. Zener, Proc. R. Soc. London Ser. A **137**, 696 (1932).
[7] M. V. Berry, Proc. R. Soc. London Ser. A **392**, 45 (1984).
[8] A. Shapre and F. Wilczek, *Geometric Phases in Physics* (World Scientific, Singapore, 1998).
[9] G. Moruzzi, *The Hanle Effect and Level-Crossing Spectroscopy* (Kluwer Academic, Norwell, 1991).
[10] M. Vojta, Rep. Prog. Phys. **66**, 2069 (2003).
[11] S. Sachdev, *Quantum Phase Transitions* (Cambridge University Press, Cambridge, 2001).
[12] R. G. Unanyan, N. V. Vitanov, and K. Bergmann, Phys. Rev. Lett. **87**, 137902 (2001).
[13] T. Kohler, K. Goral, and P. S. Julienne, Rev. Mod. Phys. **78**, 1311 (2006).
[14] X. J. Wu, T. X. Li, C. Zhang, and R. R. Du, Appl. Phys. Lett. **106**, 012106 (2015).
[15] G. Breit and I. I. Rabi, Phys. Rev. **38**, 2082 (1931).
[16] A. Abragam, *The Principles of Nuclear Magnetism* (Clarendon, Oxford, 1961).
[17] E. Merzbacher, *Quantum Mechanics* (Wiley, New York, 1970).
[18] S. Oh, Z. Huang, U. Peskin, and S. Kais, Phys. Rev. A **78**, 062106 (2008).
[19] M. Bhattacharya and C. Raman, Phys. Rev. A **75**, 033406 (2007).
[20] E. A. Yuzbashyan, W. Happer, B. L. Altshuler, and S. B. Shastry, J. Phys. A: Math. Gen. **36**, 2577 (2003).
[21] S. S. Gubser and R. K. Bradley, Adv. Theor. Math. Phys. **9**, 593 (2005).
[22] C. J. Erickson, D. Levron, W. Happer, S. Kadlecek, B. Chann, L. W. Anderson, and T. G. Walker, Phys. Rev. Lett. **85**, 4237 (2000).
[23] C. M. Bai, M. L. Ge, and K. Xue, Sci. China Ser. A **32**, 320 (2002).
[24] C. M. Bai, M. L. Ge, and K. Xue, Int. J. Mod. Phys. B **16**, 1867 (2002).
[25] F. Jelezko, T. Gaebel, I. Popa, A. Gruber, and J. Wrachtrup, Phys. Rev. Lett. **92**, 076401 (2004).
[26] T. A. Kennedy, J. S. Colton, J. E. Butler, R. C. Linares, and P. J. Doering, Appl. Phys. Lett. **83**, 4190 (2003).
[27] R. Hanson, O. Gywat, and D. D. Awschalom, Phys. Rev. B **74**, 161203(R) (2006).
[28] G. Balasubramanian *et al.*, Nature (London) **455**, 648 (2008).
[29] M. W. Doherty, F. Dolde, H. Fedder, F. Jelezko, J. Wrachtrup, N. B. Manson, and L. C. L. Hollenberg, Phys. Rev. B **85**, 205203 (2012).
[30] V. R. Horowitz, B. J. Alemán, D. J. Christle, A. N. Cleland, and D. D. Awschalom, Proc. Natl. Acad. Sci. USA **109**, 13493 (2012).
[31] G. D. Fuchs, V. V. Dobrovitski, R. Hanson, A. Batra, C. D. Weis, T. Schenkel, and D. D. Awschalom, Phys. Rev. Lett. **101**, 117601 (2008).
[32] V. Jacques, P. Neumann, J. Beck, M. Markham, D. Twitchen, J. Meijer, F. Kaiser, G. Balasubramanian, F. Jelezko, and J. Wrachtrup, Phys. Rev. Lett. **102**, 057403 (2009).
[33] M. Steiner, P. Neumann, J. Beck, F. Jelezko, and J. Wrachtrup, Phys. Rev. B **81**, 035205 (2010).
[34] M. Bhattacharya and C. Raman, Phys. Rev. Lett. **97**, 140405 (2006).
[35] M. Bhattacharya and C. Raman, Phys. Rev. A **75**, 033405 (2007).
[36] J. A. Weil and J. R. Bolton, *Electron Paramagnetic Resonance-Elementary Theory and Practical Applications* (Wiley Interscience, New York, 2007).
[37] R. Maurice, R. Bastardis, C. de Graaf, N. Suaud, T. Mallah, and N. Guihéry, J. Chem. Theory Comput. **5**, 2977 (2009).
[38] A. W. Hornig and J. S. Hyde, Mol. Phys. **6**, 33 (1963).
[39] Y. Yamaguchi and N. Sakamoto, J. Phys. Soc. Jpn. **27**, 1444 (1969).
[40] P. L. Hall, B. R. Angel, and J. P. E. Jones, J. Magn. Reson. **15**, 64 (1974).
[41] F. Z. Shi, X. Kong, P. F. Wang, F. Kong, N. Zhao, R. B. Liu, and J. F. Du, Nat. Phys. **10**, 21 (2014).
[42] L. I. Schiff, *Quantum Mechanics* (McGraw-Hill, New York, 1968).
[43] R. Gilmore, *Lie Group, Lie Algebra and Some of Their Applications* (Wiley, New York, 1974).
[44] J. Q. Cheng, *Group Representation Theory for Physicists* (World Scientific, Singapore, 1989).
[45] Q. L. Jie, S. J. Wang, and L. F. Wei, J. Phys. A: Math. Gen. **30**, 6147 (1997).